6

Other Electrode and Toroid Devices

6.1 INTRODUCTION

Electrode devices have been put to many other uses than those described in Chapter 5, the earliest of these being the measurement of the resistivity of the invaded or flushed zone R_{xo}. Historically, the first use of the invaded-zone resistivity was, in the absence of any other measurement, to make an estimate of the formation porosity. Since then R_{xo} has found many applications. In earlier chapters we saw that R_{xo}, when compared with R_t, gives a visual indication of permeable zones and evidence of moved hydrocarbons. In Chapter 5 we saw the need for R_{xo} in obtaining a better estimate of the deep-resistivity R_t. R_{xo} can be combined with other information to determine the water saturation of the invaded zone, S_{xo}, and thereby estimate the efficiency of hydrocarbon recovery. S_{xo} can also be a useful indicator of hydrocarbons on its own.

Before discussing these applications, we will examine a few of the electrode devices which have been designed to measure R_{xo}. Their development has paralleled the development of laterologs, but with electrodes mounted on pads and applied against the borehole wall. Similar devices have been put to excellent use to measure the size and direction of formation dip and, later, to make detailed images of the resistivity near the borehole wall. These devices will be mentioned in this chapter but their application is primarily geological and beyond the scope of this book.

A further use for electrode devices has been on drill collars to provide logs while drilling. It is now possible to record a resistivity as soon as the bit penetrates a formation. Toroids are used instead of electrodes for current generation and focusing. The final electrode device to be considered measures the resistivity through casing. It might be thought impossible to measure resistivity through a material as conductive

as casing, but this can now be done. Indeed the measurement sees remarkably deep into the formation.

Electrodes have thus been put to a wide range of use for logging with wireline or while drilling. One word of warning: with few exceptions, electrode devices will not work in nonconductive muds, such as oil-based muds. For such muds, induction and propagation measurements are needed, as will be seen in Chapters 7–9.

6.2 MICROELECTRODE DEVICES

Microelectrode devices, as their name implies, are electrical logging tools with electrode spacings on a much-reduced scale compared to the mandrel tools previously considered. A further distinction, a result of the smaller spacings, is that their depth of investigation is also much reduced. The electrodes are mounted on special devices, called pads, which are kept in contact with the borehole wall while ascending the well.

The development of microelectrode devices has undergone the same evolution as electrode tools. The first was the microlog device (Fig. 6.1), which was an unfocused measurement based on the principle of a normal and a lateral. Current is emitted from the button marked A_0, and the potentials of the two electrodes M_1 and M_2 are measured. To ensure a shallow depth of investigation, the spacing between electrodes

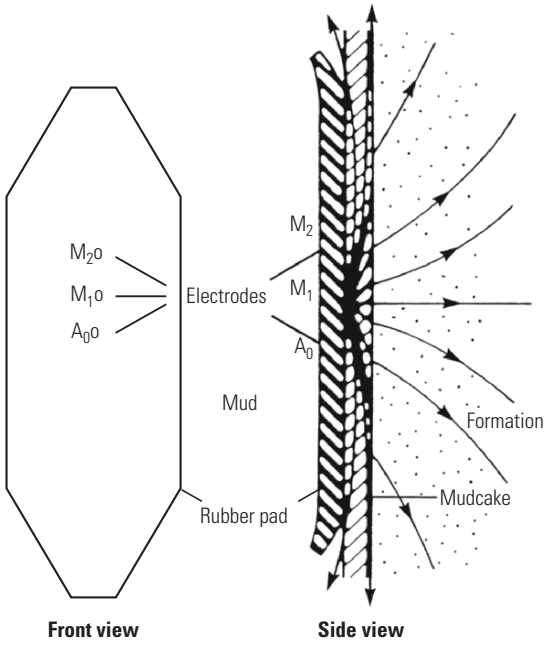

Fig. 6.1 A microlog device: a pad version of the short normal and the lateral. The spacing between the electrodes is 1 in. From Serra [1].

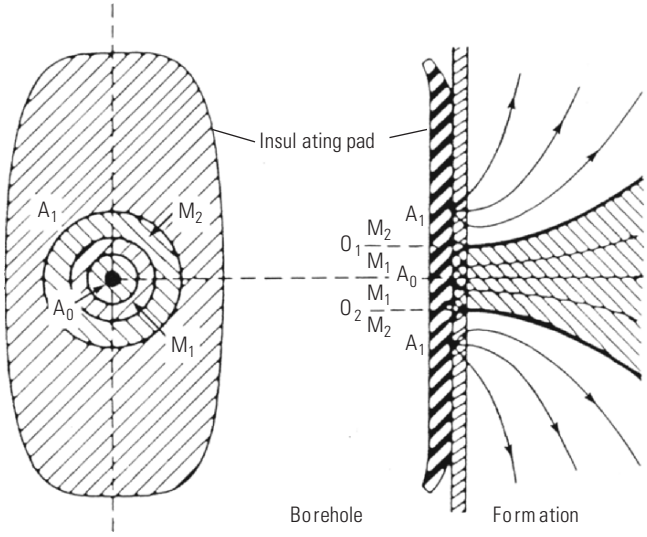

Fig. 6.2 A microlaterolog device: a reduced scale and pad version of the laterolog. From Serra [1].

is 1 in. The difference in potential between electrodes M_1 and M_2 forms a lateral, or inverse, measurement that is mostly influenced by the presence of mudcake. The potential on electrode M_2 forms a normal measurement which, being farther from the current source, is influenced more by the flushed zone.

The influence of mudcake, especially in the case of a resistive formation and a very conductive and thick mudcake, was a major disadvantage for the purpose of determining R_{xo}, but meant that the two curves separated when there was invasion. This separation proved to be a reliable indicator of permeable zones, much beloved by many log analysts, to the extent that modern tools create synthetic microlog curves just for this purpose. Examples of many microelectrode-device logs and their interpretation can be found in Jordan and Campbell [2].

In order to improve the determination of R_{xo}, a focused or microlaterolog device was the next innovation. Figure 6.2 is a schematic of this device, which shares many features of the laterolog, except for dimensions. As indicated in Fig. 6.2, the bucking current from electrode A_1 focuses the measure current to penetrate the mudcake. Depending on the contrast between R_{xo} and R_t, 90% of the measured signal comes from the first 2–4 in. of formation.

Various other microelectrode devices followed the microlaterolog, each trying to minimize the effect of mudcake while not reading too deep into the formation. The two mudcake-correction charts in Fig. 6.3 allow comparison between two types of devices – the microspherical log and the microlaterolog. The microspherical device is based on the same principle as the spherical log described in Section 5.3.2. The spherical focusing, as well as a larger pad, causes it to be much less sensitive to the presence of mudcake.

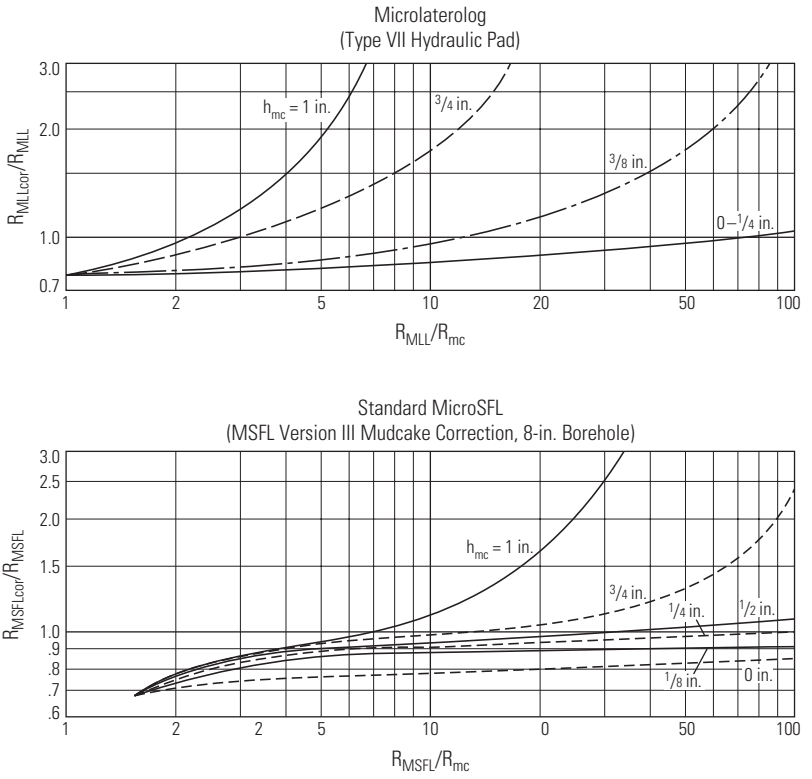

Fig. 6.3 Mudcake corrections for two types of microresistivity device. Courtesy of Schlumberger [3].

The micro-cylindrically focused log developed the measurement further [4]. It uses a rigid metal pad, unlike earlier devices that used flexible rubber pads. The rigid design prevents deformation and makes a more consistent standoff correction. The pad itself forms the guard electrode A_0 within which, and insulated from, are inserted three small measure electrodes (Fig. 6.4). The measure electrode B_0 is focused along the vertical axis by A_0 in a passive LL3-type design, with current being emitted from B_0 so as to maintain it at the same potential as A_0. The electrodes B_1 and B_2 are less focused, and therefore read shallower, because they are closer to the top edge of the pad. Focusing in the horizontal plane is more difficult because the pad's width is necessarily smaller than the pad's length, so that the area available for focusing is smaller. Horizontal focusing is therefore active, with two bucking electrodes on each side of the pad emitting the current needed to maintain the monitor electrodes at the potential of A_0. The combination of vertical and horizontal focusing ensures cylindrical equipotential lines near the center of the pad.

With three measurements of three different radial sensitivities it is possible to solve for three unknowns, R_{xo}, R_{mc}, and t_{mc}, where the latter is the mudcake thickness. The

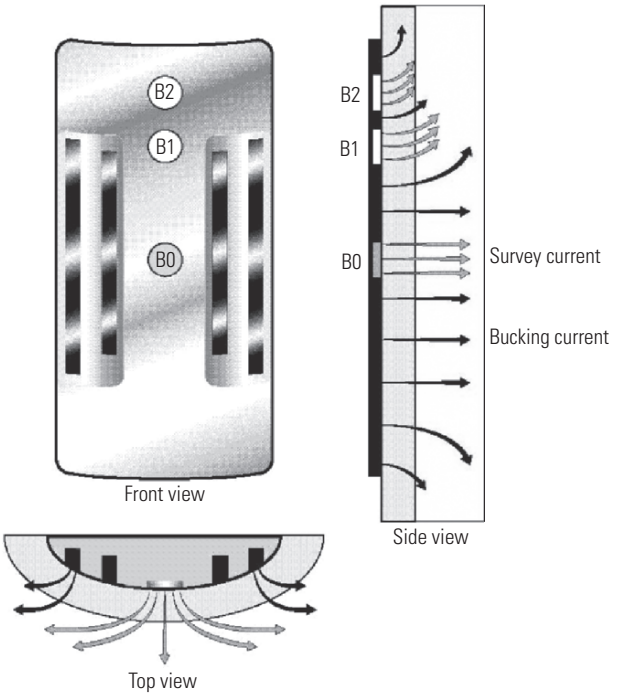

Fig. 6.4 Pad layout for the Micro Cylindrically Focused Tool. The two bars near the outer edges on each side of the pad are bucking electrodes; the inner two bars are monitor electrodes. The pad itself forms the A_0 electrode. Courtesy of Schlumberger.

solution is obtained by iterating through a forward model of the electrode responses, rather than looking up in a table as for previous devices (or in a chart if done manually). This allows more flexibility to handle different conditions and allows constraints to be added, such as that R_{mc} can only vary slowly up the borehole.

6.3 USES FOR R_{XO}

In the early years of resistivity logging, no porosity information was available from other logging devices. For this reason, the first use of R_{xo}, the estimation of porosity, is of historical interest only. This estimation is based on knowledge of the mud-filtrate resistivity R_{mf} (obtained from a mud sample) and a very shallow-resistivity measurement.

Following the definition of the formation factor F, which relates the fully water-saturated formation resistivity to the water resistivity,

$$R_o = F\, R_w\,, \tag{6.1}$$

one can write an analogous expression for the invaded zone:

$$R_{xo} = F\, R_{mf} \,. \tag{6.2}$$

Here, it is supposed that the mud filtrate of known resistivity R_{mf} has displaced the connate water. Also, by analogy, an expression for the mud-filtrate saturation of the invaded zone can be written:

$$S_{xo} = \sqrt{F\,\frac{R_{mf}}{R_{xo}}}\,, \tag{6.3}$$

where the mud-filtrate resistivity has replaced R_w in the usual formula, R_{xo} has replaced R_t, and the exponent n is assumed to be 2.

In order to get an estimate of the porosity, one can further make the assumption that the invaded zone is completely water-saturated and that the porosity dependence of F is $1/\phi^2$. From this, one obtains:

$$\frac{1}{\phi^2} = \frac{R_{xo}}{R_{mf}}\,. \tag{6.4}$$

Since the water saturation may not be complete, this can be used to obtain a lower limit to porosity, which is given by:

$$\phi \geq \sqrt{\frac{R_{mf}}{R_{xo}}}\,. \tag{6.5}$$

With porosity now measured by many other devices, the procedure above is rarely used. However R_{xo} has proved useful in many other ways. We have already seen its use for invasion corrections (Chapter 5) and for the identification of movable oil (Chapter 2). It is worthwhile investigating the latter more thoroughly by quantifying the separation often observed between the microresistivity curves, which correspond to R_{xo}, and the deep-resistivity curves, which are usually close to R_t.

From the generalized saturation equation:

$$S_w^n = \frac{a}{\phi^m}\,\frac{R_w}{R_t}\,, \tag{6.6}$$

it is possible to write an expression to compare the initial value of the water saturation (that in the uninvaded zone, S_w) to the water saturation in the invaded zone (S_{xo}). This is given by:

$$\left(\frac{S_w}{S_{xo}}\right)^n = \frac{\frac{R_w}{R_t}}{\frac{R_{mf}}{R_{xo}}} = \frac{R_w}{R_{mf}}\,\frac{R_{xo}}{R_t}\,. \tag{6.7}$$

which may also be rewritten as:

$$\frac{R_{xo}}{R_t} = \frac{R_{mf}}{R_w}\left(\frac{S_w}{S_{xo}}\right)^n\,, \tag{6.8}$$

It is clear that the ratio R_{xo}/R_t should be equal to the ratio of the mud-filtrate resistivity to the water resistivity in a water zone. The same is true if $S_{xo} = S_w$, as may happen in a zone with residual hydrocarbons that are not displaced by invasion, or in a zone with high-viscosity hydrocarbons such as tar or heavy oil. However, if there are any movable hydrocarbons, S_{xo} will be greater than S_w and the ratio R_{xo}/R_t will decrease. This ratio therefore indicates movable hydrocarbons when it decreases below R_{mf}/R_w. In practice the ratio is often formed by taking the microresistivity log as R_{xo} and the deep-resistivity log as R_t.

An example of this type of behavior can be seen in the laterolog example of Fig. 6.5. Shown is a log of the bottom 800 ft of a hydrocarbon reservoir. In zone 1 it can be assumed, in the absence of other information, that only water is present; the formation is fully water-saturated, with a shallow (MSFL) and deep-resistivity separation of about a factor of 2. Moving up to zones 2 and 3 all three resistivity curves increase. This could be due to a reduction in porosity, but if these zones were water-filled there should be the same separation between the curves as in zone 1. The reduction in ratio to about 1 clearly indicates movable oil. Moving further up the reservoir, the water saturation and hence the resistivity in the invaded zone remains roughly constant while the water saturation in the uninvaded zone becomes progressively smaller and the hydrocarbon saturation progressively greater. The ratio steadily decreases to about 1/50 in the upper part of the reservoir.

In the preceding example, we looked at relative saturations between the invaded and deep zones. However, the saturation of the invaded zone is of interest in its own right. For its determination, additional information is necessary. If the value of porosity is known from an additional measurement, then the residual oil saturation can be calculated from:

$$S_{xo}^n = \frac{a}{\phi^m}\frac{R_{mf}}{R_{xo}} . \tag{6.9}$$

This saturation can be used to determine the efficiency of water-flood production, because it quantifies the residual hydrocarbon saturation after flushing with mud filtrate. In a water flood, or a reservoir in contact with a water zone, hydrocarbons are displaced by water leaving a certain volume of residual hydrocarbon behind. The same mechanism occurs during invasion, but the rate is higher and the time shorter in the latter so that the displacement can be less efficient. The residual hydrocarbon saturation estimated from invasion, $(1 - S_{xo})$, may then be too high.

S_{xo} is also a useful indicator of hydrocarbons when the formation water salinity is variable or unknown. For example if, in Fig. 6.5 we only saw the top section of the log down to 11,900 ft, we might conclude that this was a water zone with $R_w = 50 \times R_{mf}$. But we can now calculate S_{xo} from the known R_{mf} and porosity from another log. If it is less than 1, there are hydrocarbons, although we cannot be sure whether or not they are movable. This application is particularly useful in sedimentary basins where formation waters are fresh, since when they are fresh they also tend to vary rapidly between reservoirs.

The calculations described above are often presented in the form of "quicklook" logs that are used as visual indicators of hydrocarbons. Which logs are used tends to vary with time and place. At one time "F logs" were popular [5]. These

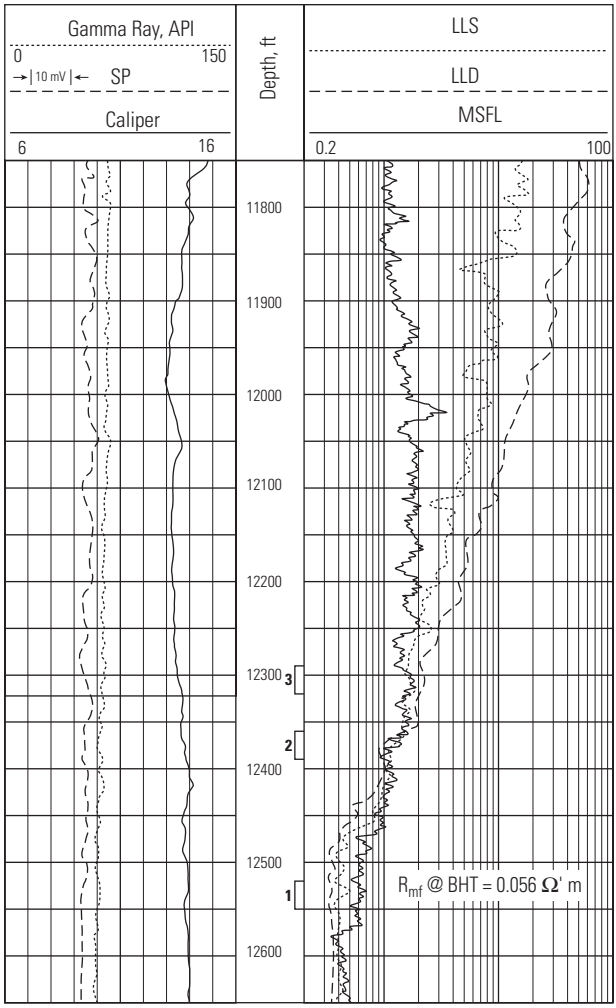

Fig. 6.5 Idealized log to be expected from a dual laterolog with a microresistivity device in a thick reservoir. The bottom zone is a water zone and the uppermost portion is hydrocarbon. A long transition zone is apparent.

were calculations of formation factor from a porosity log (e.g., $F_s = 1/\phi^2$), the microresistivity log ($F_{xo} = R_{micro}/R_{mf}$) and the deep-resistivity log ($F_t = R_{deep}/R_w$). If all three agree there is water. If $F_t = F_{xo}$ and both are higher than F_s there are residual hydrocarbons, since the calculation of F from resistivity is only valid if $S_{xo} = 1$. If $F_t > F_{xo}$ there are movable hydrocarbons.

Two commonly used quicklook logs are R_{wa} and R_{xo}/R_t. R_{wa} is the apparent water resistivity calculated from the deep resistivity and porosity assuming that $S_w = 1$, i.e., $R_{wa} = \phi^m R_{deep}$. If it is higher than the actual R_w there are

hydrocarbons. A common rule of thumb says that when $R_{wa} > 3 \times R_w$ there should be movable hydrocarbons. R_{wa} is really just the deep resistivity with porosity variations removed. In the same way the ratio R_{mfa} is a useful indicator when R_w is not known ($R_{mfa} = \phi^m R_{xo}$). The ratio R_{xo}/R_t is useful because it does not require a knowledge of porosity. As shown above this ratio will be reduced in a zone with movable hydrocarbons. An example of these curves is shown later in Fig. 23.3.

6.4 AZIMUTHAL MEASUREMENTS

The concept of small electrodes mounted on a pad was quickly extended to sondes with three or four arms, known as dipmeters. Each arm held one or more electrodes pressed against the borehole wall and sampled with a fine vertical resolution on the order of 0.1 in. Although the measurements are not necessarily calibrated in terms of resistivity, the vertical sequence of resistivity anomalies is of interest for determining the 3D orientation of strata intersecting the borehole. For a vertical well traversing horizontal layers of formation, the resistivity variations encountered by the measurement pads should correlate at the same depth. Depending on the orientation of the sonde (which is determined by an inertial platform or a magnetometer and pendulum), dipping beds will produce resistivity anomalies at different depths for each arm. The shift required to bring them into alignment will depend on the formation dip angle and borehole size.

The raw-resistivity curves of the dipmeter are rarely used directly but are subjected to various correlation or pattern recognition processing programs. These produce a summary log of the correlated events, which indicates the bedding orientation (dip angle and azimuth). The interpretation of the summary log, or "tadpole plot", in terms of structural geology and depositional environment, is beyond the scope of this book but is thoroughly treated in several references [1, 6–8].

In the 1980s the dipmeter evolved into the electrical microscanner, a device that incorporates a large number of small electrodes, or buttons, on several pads [9]. A typical pad contained 27 electrodes of 0.2 in. diameter arranged in four rows. The tool measures the current emitted by each electrode, while maintaining the potential of each electrode and the surrounding pad constant relative to a return electrode on the tool string above. The arrays of staggered electrodes are sampled at a high rate and processed to provide an electrical image of a portion of the borehole wall. Details on the scale of a few millimeters are resolved, so that the electrical image is nearly indistinguishable from a core photograph. The main drawback of early tools was that the pads did not cover a sufficient fraction of the borehole wall, particularly in large holes. Modern imaging devices contain a few hundred electrodes mounted on six arms, or else on four arms with movable flaps, so that up to 80% of the borehole wall can be covered in an 8 in. hole.

Another drawback was that the devices did not work in nonconductive muds because of the high impedance presented by the mudcake. Initially, dipmeters were fitted with sharp protruding electrodes designed to cut through the mudcake, but this was never very satisfactory. The Oil-Base Dipmeter Tool used micro-induction sensors [10], but results were sensitive to the borehole environment. Acoustic images,

described in Chapter 19, are dominated by surface effects and are poor in heavy muds. Then, beginning in 2001, new pad designs allowed images to be recorded in many nonconductive muds [11, 12]. These designs rely on the fact that both mudcake and formation do have some small conductivity due to their clay content, and that the distance between pad and formation is small. This makes it possible to send current through the formation between electrodes at the top and bottom of a pad and to measure the potential, and hence the resistivity, between buttons in the center.

Figure 6.6 compares a log from such a device with a core photograph over a 5 ft interval. On the right, the core photograph shows a sequence of thin sand and shale beds. The images on the left were obtained from four microelectrode arrays on measurement pads at different azimuths around the borehole wall. Beds as thin as 0.5

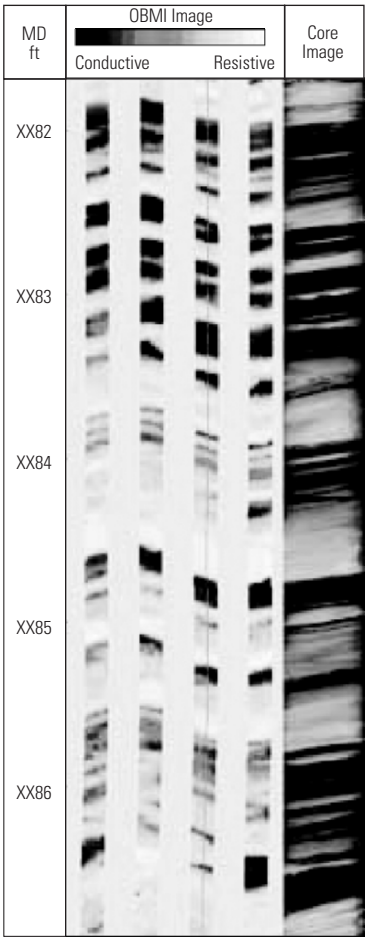

Fig. 6.6 An electrical image of the borehole produced by arrays of microelectrodes on an Oil-Base MicroImager tool laid alongside a core photograph of the same section of hole.

in. can be identified. This high resolution is very useful in the analysis of laminated sands (Section 23.3.4). Additional features such as the nonplanar bed boundary at 83.4 ft can also be seen. These images are a considerable enhancement over the conventional dipmeter measurements, which can be recorded at the same time. Bed boundaries, fractures and other events can now be picked manually from the images, and their dip and strike automatically computed. This gives an experienced geologist close control over the interpretation [13].

Images can also be obtained from azimuthal laterolog devices by sectioning one of the cylindrical current electrodes into separate segments [14]. The current emitted by each segment is adjusted so that the potential on a monitor electrode in its center is the same as that on two-ring electrodes above and below the segments. The remainder of the long-guard electrode lies above and below these electrodes, so that the whole assembly makes a monitored LL3 configuration. The resultant image is poorer than that of the microelectrode imaging tools, but can identify major structural features.

6.5 RESISTIVITY MEASUREMENTS WHILE DRILLING

The first resistivity measurement made while drilling was a short normal with electrodes mounted on an insulated sleeve, itself mounted on a drill collar. This was subsequently improved by the use of two guard electrodes in an LL3 arrangement that was also mounted on an insulated sleeve (the Focused Current Resistivity Tool, 1987 [15]). Insulated sleeves are not popular in the drilling environment as they tend to wear faster than the steel collars. A much better solution was to use toroids, as proposed by Arps in 1967 [16]. Toroids also offered a solution to the problem of measuring resistivity at the very bottom of the drill string, i.e., at the bit. It has always been highly desirable to measure the resistivity of the formation as soon as it is penetrated, or even beforehand. With this information it is possible, for example, to steer a highly deviated well within a reservoir or to stop drilling as soon as the reservoir is penetrated, as shown in the example of Fig. 6.7. These applications will be discussed in Chapter 20. In this chapter we will discuss how the measurements are made.

6.5.1 Resistivity at the Bit

The first device to measure the resistivity at the bit was the Dual Resistivity MWD Tool†, which also makes a type of lateral measurement [17]. The second device was the Resistivity at the Bit Tool (RAB*), which also makes a focused resistivity measurement [18]. A removable sleeve with button electrodes can be added to the tool in order acquire data that varies azimuthally and has different depths of investigation. An improved version of the RAB is known as the GVR*, geoVISION Resistivity sub.

†Mark of Halliburton
*Mark of Schlumberger

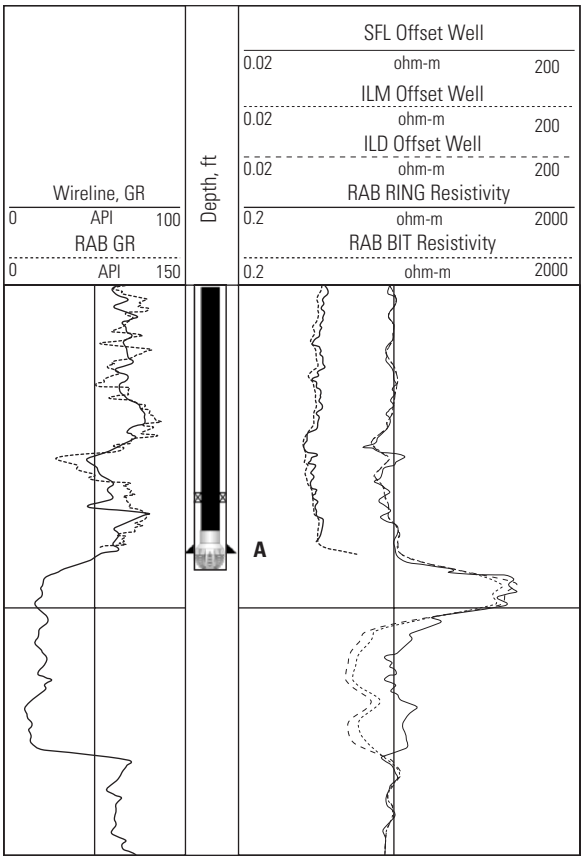

Fig. 6.7 Example of a log recorded by the RAB tool. The increase in bit resistivity at A indicates the top of the reservoir sand. This top can be seen in logs from the offset well (right). Drilling was stopped to set casing. Adapted from Bonner et al. [18]. Used with permission.

In both the Dual Resistivity MWD Tool and the RAB, a current is sent down the drill collar and out through the bit by a toroidal transmitter before returning through the formation (Fig. 6.8). The toroidal transmitter, shown in Fig. 6.9a, is a transformer with its coils acting as the primary, and the drill collar and return path through the formation acting as the secondary. A low (1,500 Hz) alternating voltage is applied to the coil inducing a voltage difference between the collar sections above and below the toroid. This voltage difference, which is almost entirely in the formation due to the low resistance of the collar, is equal to the input voltage divided by the number of turns in the toroid. The axial current is measured by a toroidal monitor (Fig. 6.9b). This is also a transformer with, in this case, the drill collar and formation acting as the primary and the coils as the secondary. The current flowing in the coils is equal to the axial current divided by the number of turns.

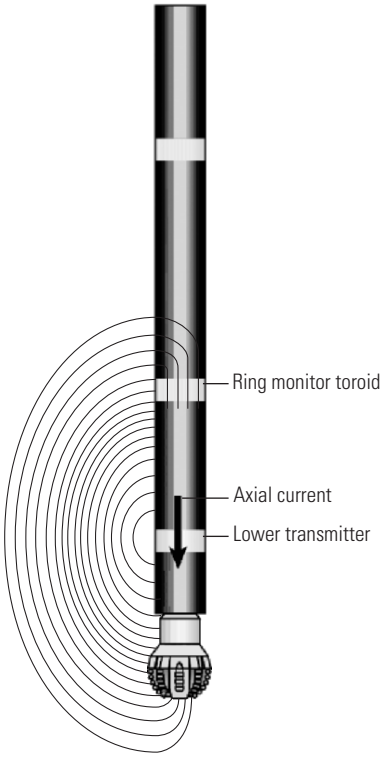

Fig. 6.8 An illustration of how resistivity is measured at the bit. The toroid transmitter sends current down the drill collar and out through the bit. The current lines that travel through the formation return further up the collar where they are measured by a monitor toroid. Courtesy of Schlumberger.

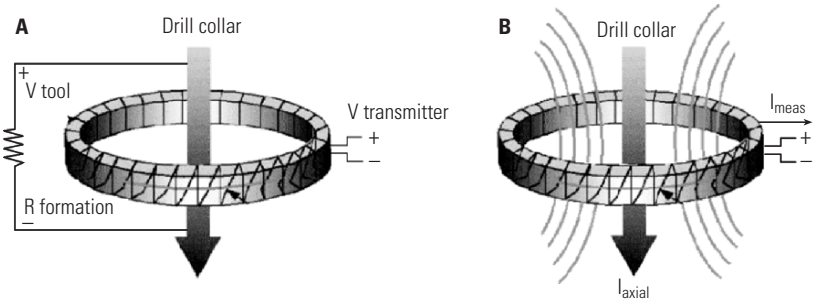

Fig. 6.9 (a) A toroidal transmitter formed by wrapping a coil around a ferromagnetic toroid. The voltage $V_{tool} = V_{transmitter}/N$, where N is the number of turns in the coil. (b) A current monitor formed by connecting a toroidal coil to a low impedance circuit. The current $I_{meas} = I_{axial}/N$. From Bonner et al. [18]. Used with permission.

It is important to maximize the amount of current flowing out through the bit but at the same time to place the transmitter and monitor far enough apart that the measured current flows through the formation and not the borehole. For this reason the transmitter is placed as close to the bit as possible and the monitor is placed further up the string (Fig. 6.8). Resistivity is calculated from:

$$R_{app} = K \frac{V_{tool}}{I_{meas}}, \tag{6.10}$$

where V_{tool} is the formation voltage drop measured by the toroid and I_{meas} is the current at the monitor. K depends on the drill collar geometry.

The result is an unfocused device whose characteristics depend strongly on the distance between transmitter and bit. When the main purpose of the log is to measure the resistivity of the formation as soon as it is penetrated, the RAB should be placed immediately above the bit. This gives a reasonable vertical response of a few feet as well as the earliest response to resistivity changes. If the RAB tool is placed further up the tool string, the response is less well-defined and the measurement is more qualitative than quantitative.

Surprisingly, this measurement works in most oil-based muds, even though they are nonconductive. The reason is that the formation is in contact with the bit as well as with some part of the drill collar, usually through a stabilizer. There is thus a current return path. However in nonconductive mud the current returning through the monitor shown in Fig. 6.8 is unpredictable, so it is measured at another monitor placed just below the transmitter (not shown). There is no concern about current flowing through the borehole in this situation.

6.5.2 Ring and Button Measurements

Horizontal (or radial) formation resistivity, such as is measured by wireline devices, is derived in the RAB from a set of ring electrodes and three button assemblies, all of which are insulated from the body of the collar (Fig. 6.10). The central ring electrode is focused using monitor electrodes in a LL7 configuration, while the button assemblies also use monitor electrodes in an arrangement similar to the microlaterolog. The resistivity seen by each electrode can then be calculated from the measure current sent by the large central ring, the voltage on the monitor electrodes and using an equation similar to Eq. 6.10.

In practice it is not quite as simple as this. First, there is some potential drop in the drill collar because it does not have infinite conductivity and because, in spite of the low-operating frequency, skin effect confines the current to a small cross section of the collar. This correction is handled by a transform for each electrode established by modeling and verified in salt water tanks. Different transforms are needed for different drill collar geometries.

Secondly, as with standard electrode devices, the use of a single transmitter and detector leads to distortion at bed boundaries (Fig. 6.11a). In other words it needs to be focused. This is achieved by adding a second transmitter and two monitor toroids (Fig. 6.11b). The upper and lower transmitter (T_1 and T_2) are driven 180° out of

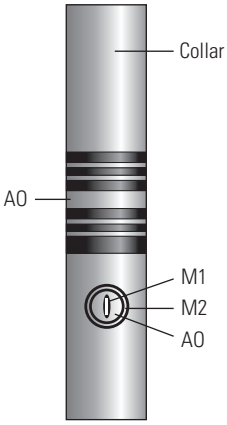

Fig. 6.10 Mounting of the ring assembly (top) and one of the button assemblies on the collar. Black parts are insulation, grey parts are conductive. The rings above and below the A_0 ring are monitor electrodes. Courtesy of Schlumberger.

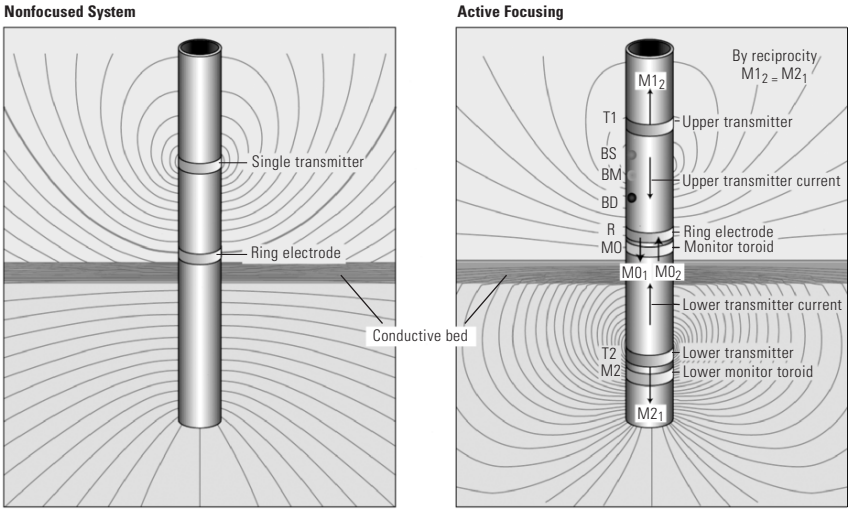

Fig. 6.11 From the simple concept to the practical device with attendant complications. Left panel: the unfocused current map that results from using a single transmitter when a conductive bed prevents the current flowing radially at the ring. Right panel: in the RAB tool, multiple transmitter and monitor toroids are used to maintain radial focusing at the ring electrode. The current lines at the ring are now nearly radial. The notation M_{01} indicates the current at M_0 due to transmitter T_1. Adapted from Bonner et al. [18]. Used with permission.

phase so that in a homogeneous formation the axial current at the ring is zero and the radial current is perpendicular to the collar. *When the formation resistivities above and below the ring are not identical this symmetry must be maintained by adjusting the outputs of T_1 and T_2. They are first adjusted so that the axial current at M_0 is zero. The ring is close enough to M_0 to also have zero axial current. This adjustment could be done in hardware by firing the transmitters simultaneously and measuring the net current at M_0. In practice it is done in software by firing the transmitters sequentially, measuring the currents that each produce at the monitor, labeled M_{01} and M_{02} in the figure, and adjusting the transmitter outputs accordingly.*

The outputs from T_1 and T_2 must be further adjusted since the current losses between T_1 and the ring can be different to those between T_2 and the ring. These losses are measured by the ratio of currents generated by T_1 at M_0 and M_2 (M_{01}/M_{21}) and by a similar ratio for T_2. This can only be done with one transmitter firing. For this reason measurements must be made alternatively from T_1 and from T_2 and both adjustments done in software. One final twist – there is no monitor toroid at the upper transmitter since by the principle of reciprocity the current M_{12} can be assumed equal to M_{21} which is already measured.

The result of focusing is that the equipotential surfaces near the ring are cylinders for a significant distance into the formation. Much effort has been put into focusing the ring, but what about the buttons? These are intended to be less focused than the ring and are therefore placed nearer one of the transmitters. As can be appreciated from the current lines in Fig. 6.11b the nearer the button is to the transmitter the less focused it is, and therefore the shallower the depth of investigation. With three buttons of different depths of investigation it is possible to make invasion corrections in the traditional manner.

6.5.3 RAB Response

The general features of RAB response are determined by the size and position of the electrodes and the fact that it is a resistivity device. Like a laterolog the RAB responds to resistivity and therefore performs best when formation resistivity is high, mud resistivity is low and $R_{xo} < R_t$. The small size of the electrodes and the proximity of the buttons to the transmitter give a vertical resolution of approximately 2 in. and shallow depths of investigation of approximately 1, 3, and 5 in. for the buttons, and 8 in. for the ring. These depths are considered sufficient to probe the shallow invasion expected at the time of logging. However, invasion can be significant when LWD logs are run, as discussed in Chapter 2.

The same types of environmental factors apply as for wireline electrode devices: borehole, shoulder bed, and invasion. RAB tools are designed for particular bit sizes, as are all drill collars and LWD tools. Providing the hole is at bit size, borehole corrections are negligible since the distance between drill collar and borehole wall is less than an inch. There are two exceptions. First, if the hole washes out, the corrections on the shallower and then the deeper measurements rapidly become significant. Second, as the ratio R_t/R_m drops below 10, the corrections also become increasingly significant. Charts for the borehole effect are available [3].

The effect of distant shoulders is small, which is not surprising considering the small electrode size and the long drill collars. There are, however some squeeze and anti-squeeze effects at bed boundaries that cause horns at large-contrast boundaries.

The most important effect by far is invasion. We saw in Fig. 5.18 that the pseudogeometric factors for the laterolog varied with the resistivity contrast R_{xo}/R_t. This is even truer for the RAB. The depths of investigation quoted above are the depths at which the pseudogeometric factor is 0.5 for the 6.75 in. diameter tool used in 8.5 in. boreholes when $R_{xo} = 10$ ohm-m and $R_t = 100$ ohm-m. If the contrast is higher the depths are less.

Although pseudogeometric factors give a convenient picture of depth of investigation, it can often be more instructive to consider the actual log reading in case of invasion. The actual reading depends on R_{xo} and R_t as well as the pseudogeometric factor (Eq. 5.16). The top panel of Fig. 6.12 shows the readings on the ring and button

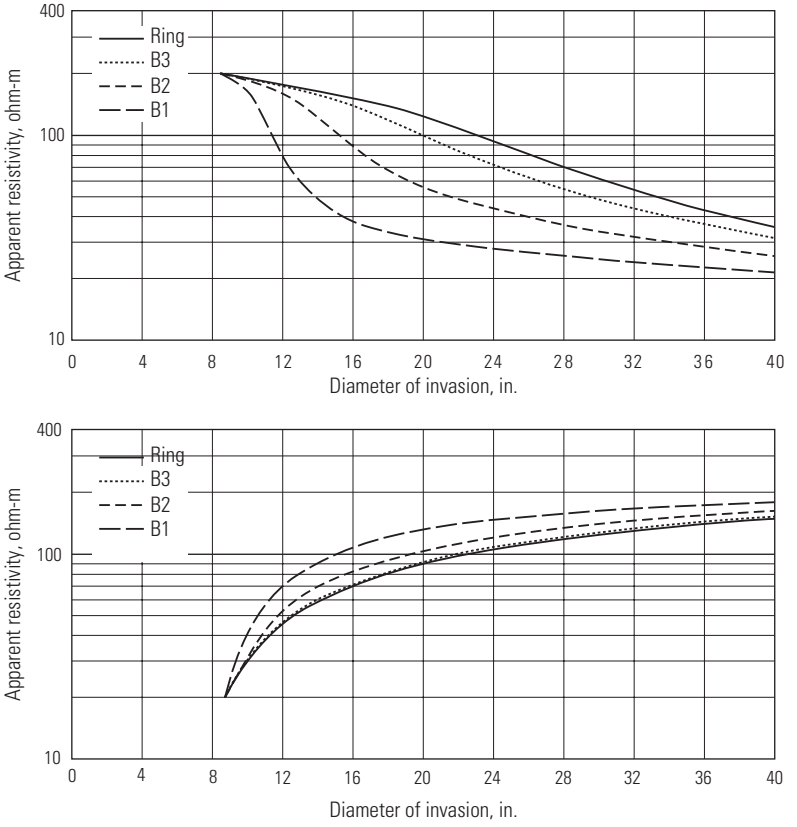

Fig. 6.12 Top panel: the apparent resistivity seen by the ring and button electrodes for a 10:1 conductive invasion and varying invasion diameter. Bottom panel: the apparent resistivity seen by the ring and button electrodes for a 10:1 resistive invasion and varying invasion diameter. Adapted from Bonner et al. [18]. Used with permission.

electrodes as invasion increases for the case where $R_{xo} = 20$ ohm-m and $R_t = 200$ ohm-m, i.e., with conductive invasion. The results are plotted in terms of diameter so that at 8.5 in. (the borehole size) there is no invasion and all measurements read R_t. As invasion diameter increases all measurements tend to R_{xo}. At an invasion diameter of 23 in., which is a depth of invasion of 7.75 in., the ring reads 50% of R_t. The large separation between the curves indicates that it will be easy to invert the logging measurements when R_t, R_{xo}, and D_i are not known. The bottom panel of Fig. 6.12 shows the opposite case of resistive invasion. Here the ring reads 50% above R_t at the very small D_i of 10 in., illustrating again that elecrode devices are not suitable with resistive invasion.

Tornado charts can be formed for a given contrast and other conditions providing there is conductive invasion. For the RAB we have the luxury of four measurements (if the sleeve with the buttons has been run). As one might deduce from Fig. 6.12a the three buttons are used when invasion is very shallow, and the two deeper buttons and the ring when invasion is deeper. More sophisticated techniques that use all four measurements are also available [19]. In Chapter 5 we saw that tornado charts are only valid for thick beds. Given the small size of the buttons and the high vertical resolution, the effect of surrounding beds and other 2D effects are much less severe than with a laterolog.

6.5.4 Azimuthal Measurements

The RAB buttons respond to the resistivity in front of them, so that if the drill string is rotated it is possible to record an image of the formation at different azimuths. This is a powerful feature as it allows images of formation features to be seen while drilling. Magnetometers orient the tool with respect to the earth's magnetic field. RAB images do not have the vertical resolution of electrical microscanners but do reflect bedding and structural features from which formation dip can be determined. This information can be very useful in near real time. For example, in highly deviated wells an image can determine whether a new bed is being entered from above or below, something that cannot be done with non-azimuthal measurements. An example of this is given in Chapter 20.

6.6 CASED-HOLE RESISTIVITY MEASUREMENTS

The ability to measure water saturation through casing is highly desirable, mainly in old wells to monitor changes with depletion and identify zones that still have producible oil. It has been done for many years using pulsed neutron devices (Chapter 15). However these have relatively shallow depths of investigation and do not always give satisfactory answers. At first sight it would seem impossible to measure resistivity through the highly conductive casing, but the method has been recognized for years, with the first patent being filed in the 1930s [20]. The main difficulty is the extremely small electrical potential that must be measured, but this was overcome in two devices

that appeared in the late 1990s: the Through Casing Resistivity Tool and the Cased-Hole Formation Resistivity Tool [21, 22].

Both tools work on the same basic principle (see Fig. 6.13). In the current leakage mode, current is sent between a downhole injection electrode and the surface. This current flows down the casing past three voltage-measuring electrodes A, B, and C, each 2 ft apart. Although most of the current stays within the casing, a small fraction leaks into the formation (ΔI). This leakage is seen as a progressive reduction in current flowing in the casing, which leads to a different potential drop from A to B than from B to C. This difference also depends on the casing resistance from A to B and B to C. If it is the same then $V_2 - V_1$ is a direct measure of ΔI, but since we are dealing with very small voltages any small difference in casing resistance is important. This difference, ΔR_c, is therefore measured in a second "calibrate" mode, in which the current is returned downhole instead of to the surface. In this configuration the leakage current is found to be negligible so that $V_2 - V_1$ is a direct measure of ΔR_c.

The signal to noise ratio is low enough that measurements must be made with the tool stationary. Logging speed is therefore slow, so there have been several efforts to speed it up. By adding a fourth electrode and duplicating circuits it is possible to make measurements at two depths, 2 ft apart, during one station. In a recent tool the two modes are performed at the same time [23]. This is achieved by a voltage generator that feeds back current around the calibrate path during the current leakage mode so as to cancel the voltage V_2. The computation now no longer depends on ΔR_c but on

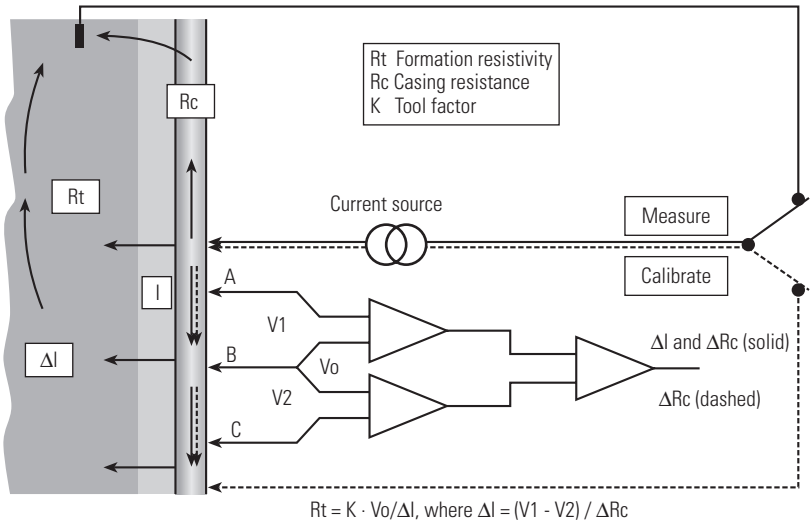

Fig. 6.13 The basic principle of measuring resistivity through casing. The formation current, ΔI, and the variation in casing resistance between AB and BC, ΔR_c, are measured in two steps, labeled Measure and Calibrate. In some later tools more complex circuitry allows this to be done in one step. From Beguin et al. [22]. Used with permission.

V_1 and the R_c between A and B. The latter can be measured at the same time as, but with a different frequency than, the current leakage. The result is a reduced sensitivity to measurement errors and a one-step, faster, recording.

With the formation current ΔI known, R_{app} can be calculated from Eq. 6.10 with the voltage on the casing at the electrodes, V_0, and a K-factor. V_0 is measured by sending current as in the current leakage mode and measuring the voltage between the downhole voltage electrodes and a surface reference (not shown in Fig. 6.13). Although V_0 varies slowly with depth it is not easy to measure accurately because it is small (less than 100 mV) and because of problems with the surface reference electrode: for example, it may not be possible to place the electrode far enough from the casing to be considered at zero potential. In practice cased-hole resistivity logs may need to be shifted to match openhole logs in a shale or other zone where formation resistivity should not have changed with time. Any such shift needs to be adjusted near the bottom of the casing where voltage changes fast with depth.

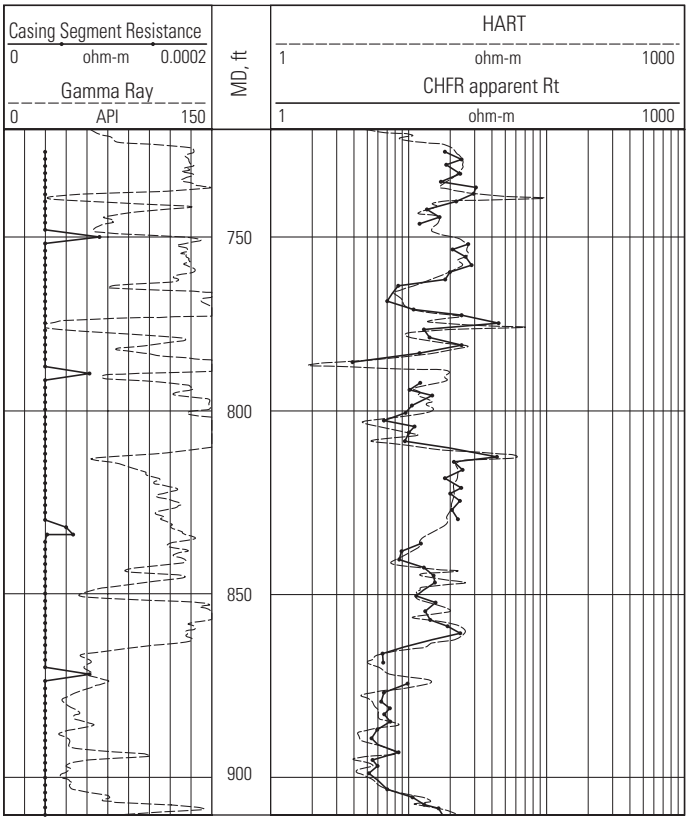

Fig. 6.14 A cased-hole formation resistivity log in a newly cased well versus a laterolog previously recorded in the open hole. From Beguin et al. [22]. Used with permission.

Understandably there are some limitations to the through-casing measurement. First we should appreciate that formation resistivity is typically nine orders of magnitude larger than that of the casing. However the formation presents a much larger area than the casing, so that the ratio of resistances and hence of leakage current to total current is around 10^{-4}. This current is measured through a casing resistance that is a few tens of micro-ohms, leading to a differential voltage $V_2 - V_1$ that is in nanovolts. In order to achieve sufficient signal to noise, this small voltage must be measured over a period of time with the tool stationary. The measurement frequency is no more than a few Hz: at higher frequencies the skin depth in the casing would be reduced, confining even more of the current within the casing and further decreasing the leakage current, while a direct current would polarize and drift.

For the time being the tool works best in the formation resistivity range 1 ohm-m to 100 ohm-m. Below 1 ohm-m the measurement becomes sensitive to the cement resistivity and thickness, neither of which are well known. As resistivity increases, the formation current drops. This can be partially overcome by repeating the measurement for a longer period at each station, but there is a practical limit on how much this can be done. The good agreement that can be obtained within the 1–100 ohm-m range between cased-hole resistivity and an openhole laterolog can be seen in Fig. 6.14.

Once measured, the resistivity through casing has some appealing features. The casing acts as a giant guard electrode so that the leakage current is particularly well focused. In an infinitely thick formation the depth of investigation is of the order of tens of feet, much larger than a laterolog. Like any laterolog, this is reduced in thinner beds. Also like a laterolog, an invaded zone or cement that is more resistive than R_t affects strongly the measurement.

REFERENCES

1. Serra O (1984) Fundamentals of well-log interpretation. Elsevier, Amsterdam, The Netherlands

2. Jordan JR, Campbell FL (1986) Well logging II – electric and acoustic logging. SPE Monograph Series, SPE, Dallas, TX

3. Schlumberger (2005) Log interpretation charts. Schlumberger, Houston, TX

4. Eisenmann P, Gounot M-T, Juchereau B, Trouiller J-C, and Whittaker SJ (1994) Improved R_{xo} measurements through semi-active focusing. Presented at the 69th SPE Annual Technical Conference and Exhibition, paper SPE 28437

5. Schlumberger (1989) Log interpretation principles/applications. Schlumberger, Houston, TX

6. Schlumberger (1970) Fundamentals of dipmeter interpretation. Schlumberger, New York

7. Serra O (1985) Sedimentary environments from wireline logs. Schlumberger, New York

8. Doveton JH (1986) Log analysis of subsurface geology, concepts and computer methods. Wiley, New York

9. Ekstrom MP, Dahan CA, Chen MY, Lloyd PM, Rossi DJ (1986) Formation imaging with microelectrical scanning arrays. Trans SPWLA 27th Annual Logging Symposium, paper BB

10. Adams J et al. (1989) Advances in log interpretation in oil-base mud. Oilfield Rev. 1(2):22–38

11. Cheung P et al. (2002) A clear picture in oil-base muds. Oilfield Rev. winter 2001/2002:2–27

12. Lofts J, Evans M, Pavlovic M, Dymmock S (2003) New microresistivity imaging device for use in non-conductive and oil-based muds. Petrophysics 44(5):317–327

13. Luthi S (2001) Geological well logs: their use in reservoir modeling. Springer, Berlin

14. Smits JW, Benimeli D, Dubourg I, Faivre O, Hoyle D, Tourillon V, Trouiller JC, Anderson BI (1995) High resolution from a new laterolog with azimuthal imaging. Presented at the 70th SPE Annual Technical Conference and Exhibition, paper 30584

15. Evans HB, Brooks AG, Meisner JE, Squire RE (1987) A focused current resistivity logging system for MWD. Presented at the 62nd SPE Annual Conference and Exhibition, Dallas, paper 16757

16. Arps JJ (1967) Inductive resistivity guard logging apparatus including toroidal coils mounted in a conductive stem. US patent No 3,305,771

17. Gianzero S, Chemali R, Lin Y, Su S, Foster M (1985) A new resistivity tool for measurement while drilling. Trans SPWLA 26th Annual Logging Symposium, paper A

18. Bonner S, Bagersh A, Clark B, Dajee G, Dennison M, Hall JS, Jundt J, Lovell J, Rosthal R, Allen D (1994) A new generation of electrode resistivity measurements for formation evaluation while drilling. Trans SPWLA 35th Annual Logging Symposium, paper OO

19. Li Q, Rasmus J, Cannon D (1999) A novel inversion method for the interpretation of a focused multisensor LWD laterolog resistivity tool. Trans SPWLA 40th Annual Logging Symposium, paper AAA

20. Alpin LM (1939) The method of the electric logging in the borehole with casing. U.S.S.R. Patent No 56026

21. Maurer HM, Hunziker J (2000) Early results of through casing resistivity field tests. Trans SPWLA 41st Annual Logging Symposium, paper DD

22. Beguin P, Benimeli D, Boyd A, Dubourg I, Ferreira A, McDougall A, Rouault G, and van der Wal, P (2000) Recent progress on formation resistivity measurement through casing. Trans SPWLA 41st Annual Logging Symposium, paper CC

23. Benimeli D, Levesque C, Rouault G, Dubourg I, Pehlivan H, McKeon D, Faivre O (2002) A new technique for faster resistivity measurements in cased holes. Trans SPWLA 43rd Annual Logging Symposium, paper K

Problems

6.1 Using the SP and resistivity fundamentals, show that the following relation holds for clean formations:

$$SP = -K\left[log_{10}\frac{R_{xo}}{R_t} + 2\,log_{10}\frac{S_{xo}}{S_w}\right]. \tag{6.11}$$

6.2 A section of sandstone reservoir was logged and found to have a porosity of 18%. The water resistivity is estimated to be 0.2 ohm-m, and R_t was measured to be 10 ohm-m.

6.2.1 What is the water saturation?

6.2.2 What error in S_w (in saturation units) is induced by a 10% relative uncertainty for each of the three parameters?

6.3 Given the log of Fig. 6.5 with R_{mf} indicated at formation temperature, answer the following:

6.3.1 Over the zone 11,800–12,200 ft, what is the average value of the lower limit to porosity which can be established?

6.3.2 Evaluate S_w every 50 ft over the above interval and make a linear plot of S_w versus depth.

6.3.3 The actual average porosity over the zone in question is 30 p.u. How does this compare with your estimate? Is this discrepancy reasonable? How does this additional information impact the actual value of S_w along the zone (replot curve)?

6.4 In the bottom section of the well studied in question 6.3, assume that the porosity is constant at 30% over the entire interval and answer the following:

6.4.1 In the zones marked 1, 2, and 3, determine the corrected values of R_{LLd} and the diameter of invasion.

6.4.2 Estimate the value of R_w in this reservoir.

6.5 In the same well (Fig. 6.5) calculate the value of R_{xo}/R_t at 12,550, 12,450, 12,400, 12,200 and 11,800 ft. Use the results to identify intervals of water, residual oil, and movable oil. Calculate S_w using the value derived for R_w in the last question and the often-used empirical relation $S_{xo} = S_w^{0.2}$.

6.6 A common rule of thumb is that when $R_{wa} = 3 \times R_w$ or greater there are movable hydrocarbons. Assuming $m = n = 2$ what S_w does this correspond to?

6.7 At what diameter of invasion does the J-factor equal 0.5 for the ring electrode in the top and bottom panels of Fig. 6.12? In which of these cases would you say that the ring reads deeper?